Available online at www.sciencedirect.com

SciVerse ScienceDirect

Ceramics International 38 (2012) 5605–5611

CERAMICS INTERNATIONAL

www.elsevier.com/locate/ceramint

Structural characteristics and electrical properties of copper doped manganese ferrite

L.M. Salah [a], A.M. Moustafa [b,*], I.S. Ahmed Farag [b]

[a] Physics Department, Faculty of Science, Cairo University, Egypt

[b] Solid State Department, Physics Division, National Research Centre, Dokki, Giza, Egypt

Received 22 January 2012; received in revised form 14 March 2012; accepted 2 April 2012

Available online 12 April 2012

Abstract

A series of $Mn_{1-x}Cu_xFe_2O_4$ ferrite samples with $0.2 \leq x \leq 0.5$ were prepared using the co-precipitation method. X-ray analysis confirmed the formation of single phase cubic spinel structure for all concentrations. Rietveld refinement revealed that the $Mn_{1-x}Cu_xFe_2O_4$ with all concentrations of x belongs to normal spinel structure. The lattice parameters decrease leading to the increase in the X-ray density with increasing the copper concentration and this may be due to the difference in the ionic radii between Mn^{2+} and Cu^{2+}. The decrease in the crystallite size with increasing the copper content is attributed to the higher formation temperature. The IR absorption spectra analyses were used for the detection and confirmation of the chemical bonds in spinel ferrites. The AC electrical conductivity, real part of the dielectric constant and the loss tangent tan δ were studied as a function of the applied frequency and temperature. It was found that the AC electrical conductivity increased with increasing temperature, this increase may be related to the increase in the drift mobility of the charge carriers, which are localized at ions or vacant sites. The AC conductivity increases with increasing copper concentration which may be ascribed to the decrease in hopping length. The dielectric constant ε' and dielectric loss showed a decrease with increasing frequency and increase with increasing temperature for all compositions. The dielectric behavior is explained by using the mechanism of polarization process.

Keywords: A. Powders: solid state reaction; B. X-ray methods; C. Ferrite; C. Electrical properties

1. Introduction

Among the magnetic materials used in modern electronic engineering the ferrites with a spinel structure are the most interesting from the scientific and applied points of view [1]. The functional properties of ferrospinels depend on their composition, magnetic features and valence state of ions and also on their distribution in the real structure. In general spinels are represented by AB_2O_4, where "A" may be any divalent cation such as Mn^{2+}, Zn^{2+}, Ni^{2+}, Fe^{2+} etc. and "B" denoted trivalent cation such as Fe^{3+}, Mn^{3+}, etc. Spinels commonly adopt a cubic symmetry with the *Fd*3*m* space group, in which A^{2+} and B^{3+} cations occupy either the octahedral sites or the tetrahedral sites depending on their affinity for these various environments. When all the divalent cations are located in the tetrahedral sites, the spinel network is defined as a normal one or a direct one. In some cases, octahedral sites can also be occupied by a fraction or the totality of divalent cations, forcing an equivalent amount of trivalent cations to occupy tetrahedral sites. In such cases, the spinel structure is partially inverted or fully inverted, respectively [2]. This so-called cation distribution depends on the chemical composition and the preparation method.

Manganese ferrites belong to a group of soft ferrite materials characterized by high magnetic permeability and low losses. These materials are extensively used in many applications such as microwave devices, computer memory chips, magnetic recording media, radio frequency coil fabrication, transformer cores, rod antennas and many branches of telecommunication and electronic engineering [3–8]. The structural, electrical and magnetic properties of spinel ferrites depend upon the method of preparation, the nature of the dopant and the dopant concentration.

In the present work, four different compositions of manganese-copper ferrites have been prepared by the co-precipitation method with the chemical formula $Mn_{1-x}Cu_xFe_2O_4$, $0.2 \leq x \leq 0.5$

* Corresponding author. Tel.: +20 2 01067026289.
E-mail address: aishamous@yahoo.com (A.M. Moustafa).

0272-8842/$36.00
http://dx.doi.org/10.1016/j.ceramint.2012.04.001

and their electrical properties were studied from room temperature to 700 K in order to correlate the structural characteristics based on cation distribution and their electrical properties.

2. Experimental

The proposed ferrite was prepared by co-precipitation method using pure materials: copper nitrates, iron nitrates hexahydrates, and manganese nitrate solution in molar ratios. These materials were dissolved in distilled water separately and then added together. After that one mole of NaOH was dissolved in 1 L of distilled water and added to the dissolved salts slowly with vigorous stirring till all metal cations precipitated. The precipitate was filtered and washed with distilled water and allowed to dry in Muffle Furnace at 80 °C. This method was successfully used to prepare samples with the chemical formula, $Mn_{1-x}Cu_xFe_2O_4$, $0.2 \leq x \leq 0.5$.

The prepared samples were heated in a furnace at 1250 °C for 24 h and checked by the X-ray diffraction to insure the formation of the required chemical formula. It was found that only two concentrations consist of one phase; $x = 0.4$ and 0.5. This indicates that the other concentrations $x = 0.2$ and $x = 0.3$ need more heat treatment. The other concentrations were heated again at different temperatures and checked by X-ray diffraction; then one phase structure was obtained at 1350 °C for 12 h for other concentration.

X-ray powder diffraction data of $Mn_{1-x}Cu_xFe_2O_4$ solid solutions were recorded at ambient condition in step scanning mode using a computer controlled X-ray diffractometer (formally made by Diano corporation, USA) with Fe-filtered CoKα (λ = 1.79026 Å) radiation operated at 10 mA and 45 kV. The powder diffraction patterns were scanned in the 2θ range of 20–100°, with scan step 0.02°, and counting time 5 s/step. Annealed quartz sample was used as an external standard material for determining the zero shift and the instrumental profile under exactly the same conditions of step scanning mode conducted for the investigated samples.

The infrared patterns were recorded using Infrared spectrophotometer (Perkin-Elmer 1430) in the range 200–1000 cm^{-1}. The samples were prepared in the form of pellets in the KBr medium, the ratio of KBr to the specimen was kept at 1:100.

The real part of the dielectric constant "ε'", AC conductivity (σ) and loss tangent angle $\tan\delta$ were recorded at different temperatures as a function of the applied frequency (100–4000 kHz) using RLC bridge model HIOKI 3531 (Japan). The samples were palletized by applying a pressure of 2 tones cm^{-2}. The thickness of the discs was about 1 mm. Pellets of the samples were then annealed at 900 °C for 2 h and cooled to room temperature. The two surfaces of each pellet were polished, coated with silver paste and checked for good conduction. A K-type thermocouple connected to a digi-sense thermometer was used to measure the sample temperature with accuracy better than ±1 °C.

3. Results and discussion

3.1. Structure characterization

The XRD pattern for the system $Mn_{1-x}Cu_xFe_2O_4$ ($0.2 \leq x \leq 0.5$) is shown in Fig. 1. Analysis of the diffraction patterns of all the samples confirmed the formation of spinel cubic structure with no extra peaks corresponding to any other phase.

Rietveld refinement implemented in FULLPROFF program [9] was started using the space group *Fd3m* in which the oxygen anions occupy position 32e, with coordinates 1/4; 1/4; 1/4, while the tetrahedral A-site at 8f,with coordinates 1/8; 1/8; 1/8, and octahedral sites occupy the positions 16c, with coordinates 1/2; 1/2; 1/2. The experimental profile was fitted by modified THOMPSON Cox-HASTING PESUDO-VOIGT function [10], the background was modeled with sixth order polynomial and the preferred orientation was modeled using March's function [11,12].

In the first step of the refinement the global parameters (instrumental profile, profile asymmetry, background, and specimen displacement) were refined. In the next step, the structure parameters (atomic coordinates, specimen profile breadth parameter, lattice parameter, displacement factors, preferred orientation and site occupancy) were refined in sequence mode. The site occupancy in the two positions (octahedral and tetrahedral sites) were constrained in order to keep the sum of the same cations in the two sites always have its stoichiometric value.

In the last cycle, when the discrepancy factor R_{wp} (R-weight patterns) has reached its global minimum value, all the parameters (global and structural) were refined simultaneously giving goodness of fit index are given in Table 1. These values indicate reliable refined structural parameters. The agreement between the observed and the calculated diffraction profiles of the sample with $x = 0.3$ as representative example of the investigated compounds is shown in Fig. 2.

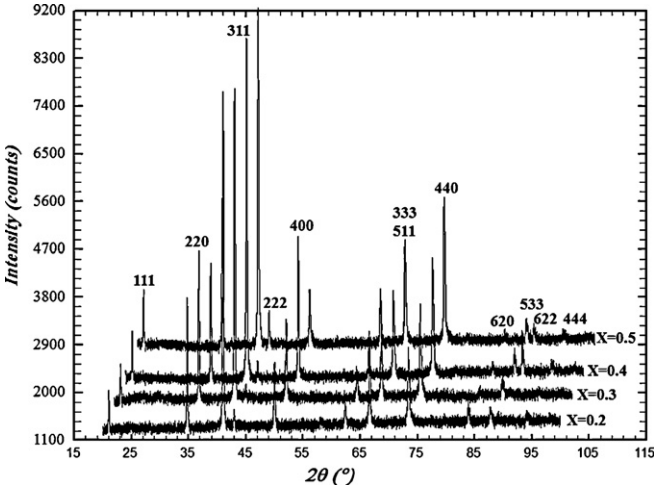

Fig. 1. X-ray powder diffraction pattern for the samples $Mn_{1-x}Cu_xFe_2O_4$ ($0.2 \leq x \leq 0.5$).

Table 1
The discrepancy factors and expected values.

Cu concentration	R_P	R_{wp}	R_{exp}	χ^2
0.2	71.7	24.6	21.1	1.36
0.3	68.2	25.1	20.01	1.57
0.4	52.3	23.1	17.6	1.723
0.5	47.6	21.4	16.7	1.639

The goodness of fit index $\chi^2 = (R_{wp}/R_{expected})^2$.

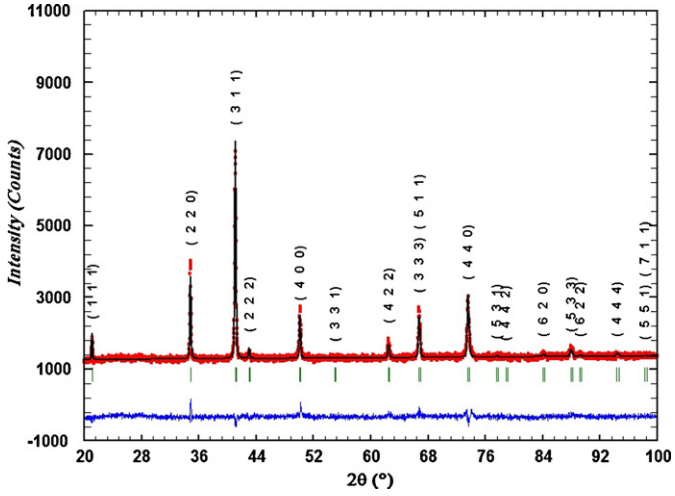

Fig. 2. The experimental and calculated X-ray patterns as well as their difference for the $Mn_{1.7}Cu_{0.3}Fe_2O_4$.

The refined values of the lattice parameters tabulated in Table 2 indicate that the values of the lattice parameters decrease from 8.452329(4) Å to 8.44046(11) Å with increasing the copper concentration and this may be due to the difference in the ionic radii between Mn^{2+} (0.66 Å) and Cu^{2+} (0.57 Å) [13]. The reduction in the physical dimension of a crystal lattice leading to a change in the lattice constants was recognized as far back as 1930, when Lennard–Jones made the conjecture that the unit cell should contract with decreasing size in ionic systems and expand in covalent ones. The results of the Rietveld analysis tabulated in Table 3 indicate, that $Mn_{1-x}Cu_xFe_2O_4$ appear to have normal spinel, that is Cu^{2+} and Mn^{2+} occupy the tetrahedral sites while the Fe^{3+} occupies the octahedral sties.

The refined values of the crystallite size decrease linearly with increasing the copper concentration as shown in Fig. 3. It is well known, that normally the increase in annealing temperature facilitates the grain growth, and enhances the coalescence process. This agrees with our findings which indicate, that the lower copper concentration samples were prepared at higher temperature than the higher concentration one. Moreover, the annealing process decreases the defect and strain results from substitution of Mn^{2+} by Cu^{2+}. This result agreed with the results obtained by Yan and Johnson [14,15] who found that the Mn^{2+} may act as slight accerlator of grain growth. Accordingly, the decrease in the crystallite size with increasing copper concentration is a normal behavior.

The values of X-ray densities tabulated in Table 2 were calculated using formula, $\rho_{xRD} = 8M/N_A a^3$ where M is the molecular weight and N_A is Avogadro's number (6.023×10^{23} atoms/mole) [16] and a is the lattice constant. From these values it is clear, that the X-ray density increases with increasing the Cu concentration because of the decrease in the molecular weight. The values of X-ray densities for our samples are comparable to those of similar compounds [17,18].

3.2. IR spectroscopy

IR spectra of the $Cu_xMn_{1-x}Fe_2O_4$, $0.2 \le x \le 0.5$ in the range (200–1000 cm^{-1}) are shown in Fig. 4. It indicates the presence of three fundamental absorption bands υ_1 (547–555 cm^{-1}), υ_2 (373–380 cm^{-1}) and υ_3 (222–223 cm^{-1}) which are found in the expected range for a spinel type ternary oxide.

Table 2
Values of the lattice parameter, unit cell volume, molecular weight calculated density, and hopping length for the compounds $Mn_{1-x}Cu_xFe_2O_4$ ($0.2 \le x \le 0.5$).

Cu content	Lattice parameter a (Å)	Unit cell volume (Å^3)	Formula sum	Formula weight (gmol^{-1})	Calculated density (g cm^{-3})	Hopping length (Å)
0.2	8.45233(4)	603.850(4)	$Cu_{1.\ 6}Mn_{6.4}\ Fe_{16}O_{32}$	1858.81	5.11127(4)	2.98835(4)
0.3	8.45091(3)	603.546(4)	$Cu_{2.\ 4}Mn_{5.6}\ Fe_{16}\ O_{32}$	1865.70	5.13279(4)	2.98785(3)
0.4	8.44139(5)	601.510(7)	$Cu_{3.\ 2}Mn_{4.8}\ Fe_{16}\ O_{32}$	1872.58	5.16919(7)	2.98448(5)
0.5	8.44046(11)	601.310(14)	$Cu_4\ Mn_4\ Fe_{16}\ O_{32}$	1879.47	5.18991(14)	2.98415(11)

Table 3
Values of atomic coordinates (x, y, z), occupancy (g) for the compounds $Mn_{1-x}Cu_xFe_2O_4$ ($0.2 \le x \le 0.5$).

Atom	$x = 0.2$		$x = 0.3$		$x = 0.4$		$x = 0.5$	
	$x = y = z$	g	$x = y = z$	g	$x = y = z$	g	$x = y = z$	g
O	0.2589(2)	4.0	0.2575(2)	4.0	0.2587(2)	4.0	0.26200(2)	4.0
Fe	0.5	2.0	0.5	2.0	0.5	2.0	0.5	2.0
Fe	0.125	0.0	0.125	0.0	0.125	0.0	0.125	0.0
Mn	0.125	0.8	0.125	0.7	0.125	0.6	0.125	0.5
Cu	0.125	0.2	0.125	0.3	0.125	0.4	0.125	0.5

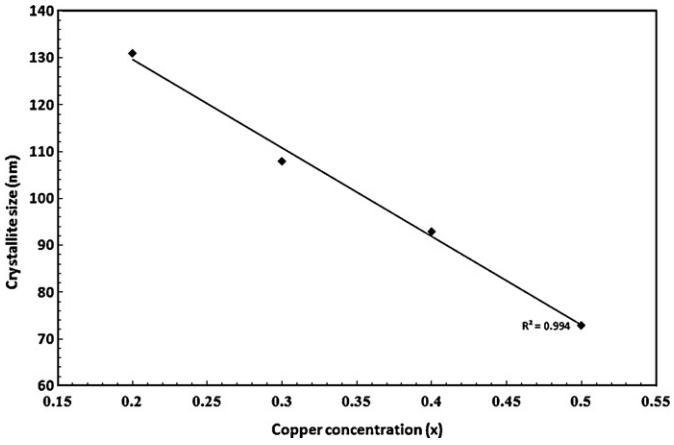

Fig. 3. Variation of the refined crystallite size with copper concentration.

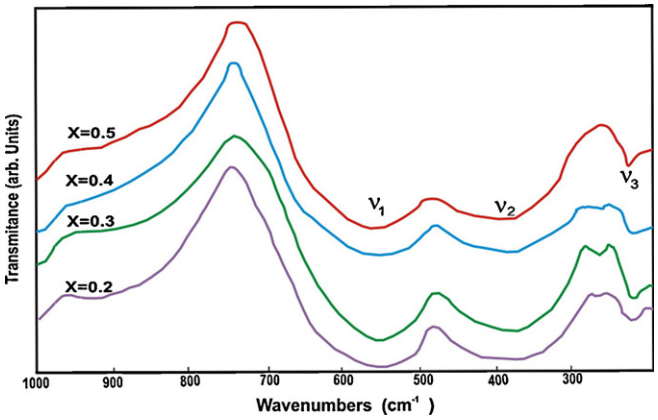

Fig. 4. IR spectra of the $Mn_{1-x}Cu_xFe_2O_4$, $0.2 \leq x \leq 0.5$ in the range (200–1000 cm^{-1}).

The band υ_1 and υ_2 should be assigned to be the intrinsic stretching vibration of the tetrahedral and octahedral complexes bonds respectively [19,20]. It is known that the frequency is inversely proportional to reduced mass and bond length. From Table 4, it is clear, that the two band υ_1 and υ_2 slightly increase with increasing Cu^{2+} concentrations. The slight increase of υ_1 with increasing Cu^{2+} may be not only due to the difference in the ionic radius between Cu^{2+} and Mn^{2+} but also due to the difference of their masses in the A-site. While, the small variation of υ_2 on these compositions can be connected with the small variation of oxygen parameter (see Table 3).

Table 4 shows that, υ_3 band is almost constant for all compositions, this behavior was observed in many studies [21,22] regardless of the ferrite type. This band is probably the characteristic of the bending vibration involving Fe^{3+} and O^{2-} of octahedral complexes as predicted by Shebanova [23].

Table 4
IR bands for the compounds $Mn_{1-x}Cu_xFe_2O_4$ ($0.2 \leq x \leq 0.5$).

Cu content	υ_1 (cm^{-1})	υ_2 (cm^{-1})	υ_3 (cm^{-1})	υ_4 (cm^{-1})
0.2	547(±4)	373(±4)	223(±4)	–
0.3	553(±4)	378(±4)	222(±4)	–
0.4	554(±4)	379(±4)	222(±4)	–
0.5	555(±4)	380(±4)	223(±4)	–

3.3. Electrical properties

Fig. 5 is a typical curve correlating AC conductivity $\ln(\sigma)$ versus absolute temperature as a function of the applied frequency for $x = 0.4$. From this figure it is clear, that $\ln(\sigma)$ increases with increasing temperature, which is a normal characteristic of semiconductor ferrites. This result agrees well with the observation of many authors [24–28]. However, the increase in conductivity with increasing temperature may be related to the increase in the drift mobility of the charge carriers, which are localized at ions or vacant sites, moreover due to the lattice vibrations, the ions occasionally come close enough for the transfer of charge carriers and the conduction induced by the lattice vibrations. Also from this figure it is clear, that the behavior of $\ln(\sigma)$ versus $1000/T$ is divided into two temperature regions: the first is ferrimagnetic region ($T < 500$ K) and the second is paramagnetic region ($T > 500$ K). The conductivity at higher temperature seems to be frequency independent and temperature dependent, while at low temperature region the conductivity is both frequency and temperature dependent. By increasing frequency, the conductivity increases as a result of the pumping force caused by the applied frequency which helps in transferring the charge carriers between the different conduction states.

Fig. 6 shows the relation between AC conductivity $\ln(\sigma)$ and copper content at constant frequency (600 kHz) and different temperatures (273 K, 573 K and 673 K). From the figure it is clear, that the conductivity increases as copper content increases. This may be explained on the basis of the conductivity in ferrites which occurs as a result of electron hopping between ions of the same element existing in different valence states on equivalent lattice sites [29,30]. The probability of electron hopping between Fe^{2+} and Fe^{3+} states is greater at the B sites due to the smaller distances between the

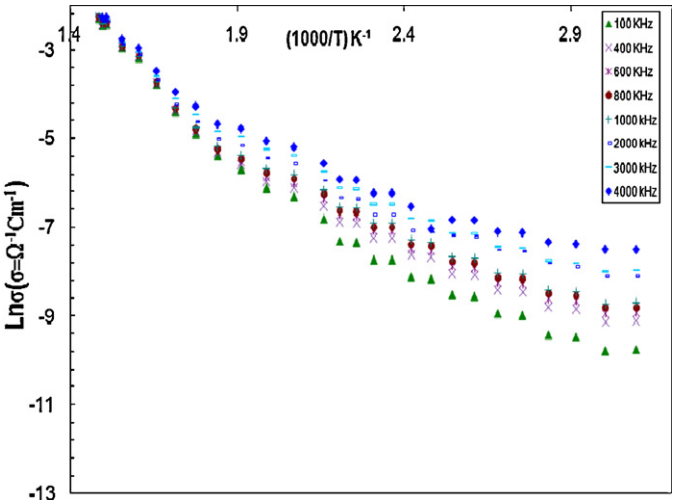

Fig. 5. Dependence of the AC conductivity on the reciprocal absolute temperature for $Mn_{0.6}Cu_{0.4}Fe_2O_4$ as a function of the applied frequency.

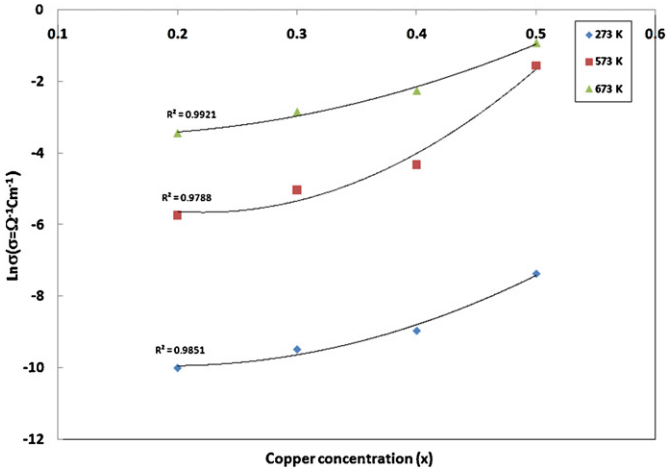

Fig. 6. Relation between AC conductivity and copper concentration at constant frequency 600 kHz and different temperatures for $Cu_xMn_{1-x}Fe_2O_4$,$0.2 \leq x \leq 0.5$.

metallic ions at these sites. X-ray confirmed this speculation, that the system $Cu_xMn_{1-x}Fe_2O_4$, $0.2 \leq x \leq 0.5$ is a normal spinel, i.e. the numbers of the electrons which jump from ferric to ferrous ions is constant for all concentrations of Cu (at the same frequency and temperature). Hence, the slight increase in the conductivity may be attributed to the decrease in the lattice parameter with increasing Cu content and in turn the hopping length L (B–B distance) will decrease according to the relation: $L = (a(2)^{0.5}/4)$ [31,32], which may cause the increase in the conductivity, i.e. as the hopping length decreases, the conductivity increases.

Fig. 7 reports typical curve correlating the real part of dielectric constant "ε'" versus the absolute temperature for the ferrite ($Mn_{0.6}Cu_{0.4}Fe_{2.0}O_4$) at different frequencies ranging from 100 kHz to 4000 kHz. From this figure it is clear, that the general trend at all frequencies is the increase in "ε'" with increasing temperature up to about 580 K where a peak (maximum) for each applied frequency is attained. Obviously, the values of these peaks are varying depending on the applied frequency. After these maxima, the values of "ε'" decrease sharply to reach a minimum and then increase again. The behavior of this sample with temperature can be more clarified, if the curves are divided into two temperature regions. In the first temperature region (300–400 K), a slight increase in "ε'" is observed. This means, that starting with small thermal energy given to the system can liberate small number of the localized dipoles, then the operating field accompanied with the applied frequency helps in aligning the liberated dipoles in its direction, giving rise to an increase in "ε'". The second region (400–600 K), the high thermal energy given to the system is quite sufficient to liberate most of the frozen dipoles, accordingly a maximum polarizability as well as maximum dielectric constant "ε'" can be achieved. After these main peaks, "ε'" decreases because the lattice vibration plays a significant role in disturbing the aligned dipoles, thus decreasing the polarization and consequently "ε'". After the minimum, the dielectric constant increases again as a result of another type of polarization after the main polarization vanishes. This polarization type may be expected to be Maxwell Wagner polarization, which it usually takes place in the high resistivity regions separating the conducting grains. It has been reported by some researchers [33,34], that the size of the conducting grains increases with temperature, i.e. the intergranular spacing decreases, accordingly Maxwell Wagner polarization is efficiently working in this area. From Fig. 7 also one can observe, that "ε'" decreases with increasing frequency. This means that at lower frequency the half life time of the oriented dipoles in different localized states is much greater than that at higher frequency. In other words, at higher frequency the dipoles cannot follow up the field variation accompanied with the applied frequency, resulting in a decrease in the dielectric constant.

The temperature dependence of the dielectric loss angle tan δ as a function of the applied frequency is shown in Fig. 8. From this figure it is clear, that tan δ increases on increasing temperature, because the electrical conductivity for the semiconductor ferrites increases on increasing temperature,

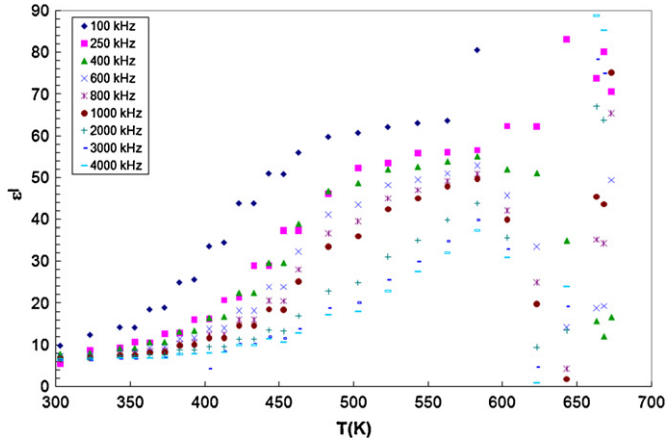

Fig. 7. Relation between real part of the dielectric constant versus absolute temperature as a function of the applied frequency for $Mn_{0.6}Cu_{0.4}Fe_2O_4$.

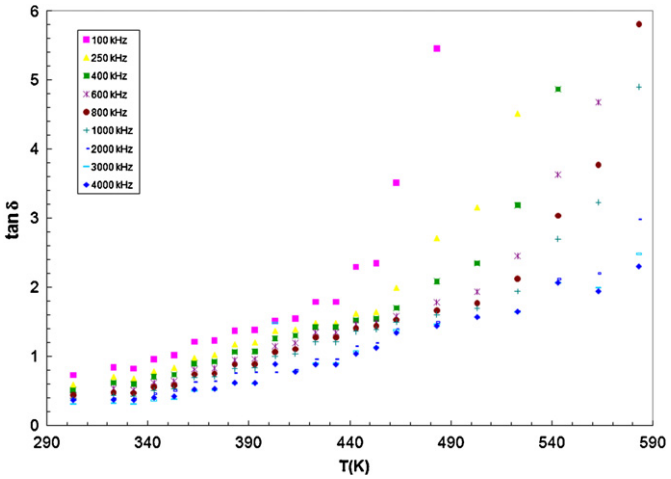

Fig. 8. Relation between dielectric loss angle tan δ versus absolute temperature as a function of the applied frequency for $Mn_{0.6}Cu_{0.4}Fe_2O_4$.

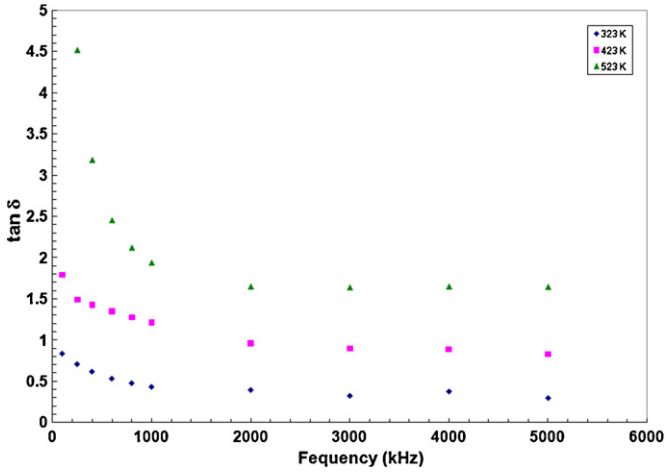

Fig. 9. Relation between dielectric loss angle tan δ versus applied frequency frequency for $Mn_{0.8}Cu_{0.2}Fe_2O_4$ at different selected temperatures.

due to the thermal activation of the charge carriers and their drift mobilities. Since the dielectric polarization in ferrites is similar to that for the electronic conduction, therefore the dielectric polarization as well as tan δ increases with increasing temperature. This foundation is consistent with the work of Ahmed et al. [35] who reported that, the dielectric losses in ferrite generally reflected in conductivity measurements where the materials of high conductivity exhibiting high losses and vice versa. It is also worth to the mention, that the rapid rise in the tan δ curve at high temperatures is attributed to the conduction losses, which increase with temperature due to increased conduction.

Fig. 9 is a typical curve correlates the relation between dielectric loss angle tan δ and frequency at some selected temperatures (323, 423 and 523 K) for the sample $x = 0.2$. The general trend of this curve is the decrease in the value of the loss angle tan δ with increasing frequency particularly at high temperature. On other hand, tan δ increases with increasing temperature and seems to be frequency independent after certain frequency. This decrease takes place when the jumping of electric charge carriers between the adjacent octahedral sites cannot follow the alternation of the applied AC field beyond a certain frequency.

4. Conclusion

1. Four compositions of manganese-copper ferrites have been prepared by the co-precipitation method with the chemical formula $Mn_{1-x}Cu_xFe_2O_4$, $0.2 \leq x \leq 0.5$.
2. X-ray analysis confirmed the formation of the single phase for the compositions $x = 0.4$ and 0.5 for the samples heated at 1250 °C for 24 h while the other concentrations $x = 0.2$ and 0.3 formed at 1350 °C for 12 h.
3. Rietveld refinement reveals that all the compositions belong to normal spinel structure, i.e. Cu^{2+} and Mn^{2+} occupy tetrahedral sites and Fe^{3+} occupies octahedral sites. The lattice parameters decreases with increasing the copper concentration and this may be due to the difference in the ionic radius between Mn^{2+} and Cu^{2+}.
4. The crystallite size decreases and the X-ray density increases with increasing copper concentration.
5. The IR spectral measurements indicate the presence of three fundamental absorption bands υ_1 (547–555 cm^{-1}), υ_2 (373–380 cm^{-1}) and υ_3 (222–223 cm^{-1}) which are found in the expected range for a spinel type ternary oxide. The slight increase of υ_1 with increasing Cu^{2+} may be not only due to the difference in the ionic radius between Cu^{2+} and Mn^{2+} but also due to the difference of their masses in the A-site.
6. The AC electrical conductivity increases with increasing temperature, which is a normal characteristic of semiconductor ferrites. This increase in the conductivity could be related to the increase in the drift mobility of the charge carriers, which are localized at ions or vacant sites.
7. The increase in copper content leads to a decrease in hopping length (L) and hence facilitates the electron hopping between Fe^{2+} and Fe^{3+} states at the B sites, and in turn leads to increase in the electrical conductivity.
8. The dielectric measurements indicate a general trend at all frequencies in which an increase in "ε'" with increasing temperature up to about 580 K where a peak (maximum) for each applied frequency is attained. The values of these peaks seem to be frequency dependent.
9. Loss angle tan δ decreases with increasing frequency when the jumping of electric charge carriers between the adjacent octahedral sites cannot follow the alternation of the applied AC field beyond a certain frequency.

References

[1] T. Abbas, Y. Khan, M. Ahmed, S. Anwar, X-ray diffraction study of the cation distribution in the Mn–Zn–ferrites, Solid State Communications 82 (1992) 701–703.
[2] M. Gaudon, N. Pailhe, A. Wattiaux, A. Demourgues, Structural defects in AFe_2O_4 (A = Zn, Mg) spinels, Materials Research Bulletin 44 (3) (2009) 479–484.
[3] E.C. Snelling, Soft Ferrites, Properties and Applications, 2nd ed., Butter Worth, London, 1988.
[4] E.C. Snelling, ICF-5: Proc. 5th International Conference on Ferrites, India, (1989), p. 579.
[5] M. Schaefer, G. Dietzmann, H. Wirth, Magnetic losses in ferrites and nanocrystalline ribbons for power applications, Journal of Magnetism and Magnetic Materials 101 (1991) 95–96.
[6] J.A.T. Taylor, S.T. Reczek, A. Rosen, Soft ferrite processing, American Ceramic Society Bulletin 74 (4) (1995) 91–94.
[7] M. Rozman, M. Drofenik, Sintering of nanosized MnZn ferrite powders, Journal of the American Ceramic Society 81 (7) (1998) 1757–1764.
[8] S.H. Chen, S.C. Chang, L.N. Lin, The influence of grain boundary internal stress on permeability: temperature curve for Mn–Zn ferrites, Journal of Magnetism and Magnetic Material 209 (2000) 193–196.
[9] J. Rodriguez-Carvajal, Short Reference Guide of the FullProf Progarm, Laboratory Leon Brillouin (CEA-CNRS), version July, 2011.
[10] P. Thomson, D.E. Cox, J.M. Hasting, Rietveld refinement of Deby–Scherrer synchrotron X-ray data from Al_2O_3, Journal of Applied Crystallography 20 (1987) 79–87.
[11] A. March, Mathematiche theorie der regelung nach der korengstalt bei affiner deformation, Zeitschrift für Kristallographie 81 (1932) 285–298.
[12] W.A. Dollase, Correction of intensities for preferred orientation in powder diffractometry: application of the March model, Journal of Applied Crystallography 19 (1986) 267–272.

[13] R.D. Shannon, Revised effective ionic radii and systematic studies of interatomic distances in halides and chalcogenides, Acta Crystallogr. A32 (1976) 751–767.
[14] F.M. Yan, D. Jonshon, Impurity-induced exaggerated grain growth in Mn–Zn ferrites, Journal of the American Ceramic Society 61 (7–8) (1978) 342–349.
[15] A.R. Bueno, L.M. Gregori, M.C.S. Nobrega, Effect of Mn substitution on the microstructure and magnetic properties of $Ni_{0.50-x}Zn_{0.50-x}Mn_{2x}Fe_2O_4$ ferrite prepared by the citrate–nitrate precursor method, Materials Chemistry and Physics 105 (2007) 229–233.
[16] M.N. Ashiq, S. Saleem, M.A. Malana, A. Ur-Rehman, Physical, electrical and magnetic properties of nanocrystalline Zr–Ni doped Mn–ferrite synthesized by the co-precipitation method, Journal of Alloys and Compounds 486 (2009) 640–644.
[17] H.M.I. Abdallah, T. Moyo, J.Z. Msomi, Mössbauer, Electrical studies of $Mn_xCo_{1-x}Fe_2O_4$ compounds prepared via glycothermal route, Journal of Superconductivity and Novel Magnetism 24 (2011) 669–673.
[18] O. Caltun, G. Rao, K. Rao, et al., The influence of Mn doping level on magnetostriction coefficient of cobalt ferrite, Journal of Magnetism and Magnetic Materials 316 (2) (2007) e618–e620.
[19] R.D. Waldron, Infrared spectra of ferrites, Physical Review 99 (6) (1955) 1727–1735.
[20] W.B. White, B.A. De Angelise, Interpretation of the vibrational spectra of spinels, Spectrochimica Acta A 23 (1967) 985–995.
[21] B. Gillot, T.D. Thiebaut, M. Laarj, Synthesis of stoichiometric cadmium substituted magnetites and formation by oxidation of solid solutions of cadmium ferrite and γ-iron oxide, Thermochimica Acta 342 (1999) 167–174.
[22] E.Z. Katsnelson, A.G. Karoza, L.A. Meleshchenko, et al., Detailed study of IR absorption spectra of manganese–zinc ferrites, Physica Status Solidi (b) 141 (1987) 599–609.
[23] O.N. Shebanova, P. Lazor, Raman spectroscopic study of magnetite ($FeFe_2O_4$): a new assignment for the vibrational spectrum, Journal of Solid State Chemistry 174 (2003) 424–430.
[24] M.A. Ahmed, M.A. El-Hiti, M.M. Mosaad, S.M. Alia, AC conductivity in Cu–Cr–ferrites, Journal of Magnetism and Magnetic Materials 146 (1995) 84–88.
[25] M.A. El-Hiti, M.A. Ahmed, M.M. Mossad, S.M. Attia, Dielectric behaviour of Cu–Cr ferrite, Journal of Magnetism and Magnetic Materials 150 (1995) 399–402.
[26] A.M.M. Farea, S. Kumar, K.M. Batoo, et al., Influence of the doping of Ti^{4+} ions on electrical and magnetic properties of $Mn_{1+x}Fe_{2-2x}Ti_xO_4$ ferrite, Journal of Alloys and Compounds 469 (2009) 451–457.
[27] M.J. Iqbal, M.R. Siddiquah, Electrical and magnetic properties of chromium-substituted cobalt ferrite nanomaterials, Journal of Alloys and Compounds 453 (2008) 513–518.
[28] I.H. Gul, A. Maqsood, Structural, magnetic and electrical properties of cobalt ferrites prepared by the sol–gel route, Journal of Alloys and Compounds 465 (2008) 227–231.
[29] A.J. Bosmann, C. Crevecoeur, Mechanism of the electrical conduction in Li-doped NiO, Physical Review 144 (1966) 763–770.
[30] R.J. Hill, J.R. Craig, G.V. Gibbs, Systematics of the spinel structure type, Physics and Chemistry of Minerals 4 (1979) 317–339.
[31] B. Gillot, F. Jemmali, Dependence of electrical properties in iron–cobalt, iron–zinc ferrites near stoichiometry on firing temperature and atmosphere, Physica Status Solidi (a) 76 (2) (1983) 601–608.
[32] M. El-Saadawy, M.M. Barakat, Effect of jump length of electrons on the physical properties of Mn-doped $Co_{0.6}Zn_{0.4}Fe_2O_4$ ferrite, Journal of Magnetism and Magnetic Materials 213 (2000) 309–311.
[33] P.K. Lareson, R. Meteselaar, Electric and dielectric properties of polycrystalline yttrium iron garnet: space-charge-limited currents in an inhomogeneous solid, Physical Review B 8 (1973) 2016–2025.
[34] S. Jankowski, Dielectric dispersion in polycrystalline ferrites: random network model, Journal of the American Ceramic Society 71 (1988) C176–C180.
[35] M.A. Ahmed, E. Ateia, L.M. Salah, A.A. El-Gamal, Structural, electrical studies on La^{+3} substituted Ni–Zn ferrites, Materials Chemistry & Physics 92 (2005) 310–321.